Quantum molecular dynamics simulations of thermophysical properties of fluid ethane

Yujuan Zhang,[1] Cong Wang,[1,2] Fawei Zheng,[1] and Ping Zhang[1,2,*]

[1]*LCP, Institute of Applied Physics and Computational Mathematics, P.O. Box 8009, Beijing 100088, People's Republic of China*
[2]*Center for Applied Physics and Technology, Peking University, Beijing 100871, People's Republic of China*

We have performed first-principles molecular-dynamics simulations based on density-functional theory to study the thermophysical properties of ethane under extreme conditions. We present results for the equation of state of fluid ethane in the warm dense region. The optical conductivity is calculated via the Kubo-Greenwood formula from which the dc conductivity and optical reflectivity are derived. The close correlation between the nonmetal-metal transition of ethane and its decomposition, that ethane dissociates significantly into molecular and/or atomic hydrogen and some long alkane chains, has been systematically studied by analyzing the optical conductivity spectra, pair correlation functions, electronic density of states, and charge density distribution of fluid ethane.

I. INTRODUCTION

Pressure-induced transformations of hydrocarbons under extreme conditions have recently drawn extensive attention and have made giant achievements in astrophysics [1]. Specifically, the planetary model with nonaxisymmetric magnetic fields generated within a thin fluid shell has successfully revealed the nonaxisymmetric nature of the Uranian and Neptunian magnetic fields [2,3]. As the interiors of these planets are composed of the fluids containing species, such as C, H, N, O, etc., the knowledge of physical properties of fluid hydrocarbons (e.g., methane, ethane, and benzene) under extreme conditions, such as equation of states (EOS), electrical conductivity, and structure, is important in this context.

Saturated hydrocarbon ethane (C_2H_6) has been reported as one of the most important decomposition products of the giant planets [4–6]. For instance, Richters *et al.* [4] have reported that ethane is formed in the decomposition process of methane at high temperature ($T = 4000$ K) and high pressure ($P \approx 100$ GPa). The observation of atmospheric ethane in Neptune, where it might be brought up from the deep interior by convection process, could be explained by the formation of ethane. Quantum molecular dynamics (QMD) simulations of Li *et al.* [5] also indicated that methane, which is a major constituent of the "ice" layer in Uranus and Neptune, mainly converts into ethane at density of 1.5 g/cm^3 along the principal Hugoniot. Meanwhile, ethane is an important fluid industrially, and the second member of the vitally interesting alkane series. Its chemical kinetics and thermophysical properties are of great interest for gas-turbine engines, high-speed propulsion, and materials synthesis [7]. Pyrolysis and oxidation of ethane have been studied behind reflected shocked waves [8]. The EOS of ethane with temperatures ranging from 90 to 625 K and pressures less than 70 MPa has been obtained by using the Benedict-Webb-Rubin equation [9]. However, such studies on ethane are limited to a narrow temperature and pressure region. More importantly, the nonmetal-metal transition (NMT) of fluid hydrocarbons is a crucial and hot topic recently. For instance, methane and benzene have been reported to transform to metallic fluids under extreme conditions, where the NMT are

associated with the rapid C-H bond breaking and the formation of atomic or molecular hydrogen [5,10]. The NMT of the system has also been found to significantly affect the optical properties, such as the reflectance and absorption coefficient. The optical reflectivity of fluid deuterium has been successfully detected in dynamic compression experiments [11]. To date, the thermophysical properties of ethane under extreme conditions have not been reported yet. Considering the present facts that (i) ethane also denotes a typical prototype and plays an important role in hydrocarbons, (ii) ethane is one of the most important decomposition products in the extreme-condition matter evolution process of the giant planets, and (iii) as a same kind of alkane species, the differences and relations of the chemical dissociation properties between methane and ethane are interesting, it is thus highly necessary to study the equation of state, chemical decomposition and recomposition picture, and electronic and optical properties of fluid ethane under extreme conditions by using an efficient method.

Materials under extreme conditions are complex, where partial dissociation, ionization, and electronic degeneration coexist. QMD simulations, based on finite-temperature density-functional theory (FT-DFT) [12], offer a powerful tool to study thermophysical properties of complex materials under such extreme conditions [13–16]. Combined with the Kubo-Greenwood formulation [17,18], the electrical and optical properties of various systems can be accurately calculated [19,20].

In the present work, we have performed QMD simulations to study the thermophysical properties of fluid ethane. By analyzing pair correlation functions, atomic structure, and charge-density distribution, we have predicted the chemical picture of the shocked ethane. In particular, the NMT for fluid ethane can be directly associated to its dissociation, which is analogous to that of molecular fluid methane. Additionally, the optical properties of fluid ethane are also discussed in the chemical picture.

II. COMPUTATIONAL METHODS

A. First-principles molecular dynamics

In this study, we have performed simulations for ethane by employing the Vienna *ab initio* simulation package (VASP)

*zhang_ping@iapcm.ac.cn

plane-wave pseudopotential code, which was developed at the Technical University of Vienna [21,22]. Electrons are fully quantum mechanically treated through solving the Kohn-Sham equations for a set of orbitals and energies within a plane-wave FT-DFT formulation [12], where the electronic states are populated according to the Fermi-Dirac distribution at temperature T_e. The ion-electron interactions are represented by a projector augmented wave pseudopotential. The exchange-correlation functional is determined by generalized gradient approximation with the parametrization of Perdew-Burke-Ernzerhof [23]. Atoms move classically according to the forces originated from the interactions of ions and electrons. The isokinetic ensemble (NVT) is employed by Nosé-Hoover thermostat [24] and the system is controlled in local thermodynamical equilibrium by setting the electron temperature T_e and the ion temperature T_i to be equal. Pseudopotentials with cutoff radius of 1.10 Bohr for carbon and hydrogen are adopted, and 650 eV plane-wave cutoff energy is employed in the simulations.

In all the simulations, a total number of 128 atoms (16 C_2H_6 molecules) are included in a supercell with periodic boundary condition. We perform finite-temperature, fixed-volume molecular dynamics simulations for selected densities ranging from 0.7 to 2.8 g/cm^3 along 3 000, 4 000, and 8 000 K isotherms. For molecular dynamic simulations, only Γ point of the Brillouin zone is included. All the dynamic simulations last 10 ps with time steps of 0.1–1.0 fs according to different conditions. For each pressure and temperature, the system is equilibrated within 1–2 ps. The isotherm equation of states data and pair correlation functions are obtained by averaging over the final 5-ps simulations for all the particles.

B. Optical and electronic properties

The electronic properties of dense ethane along isotherms are calculated in a spatial configuration of all atoms at a single time step within a MD trajectory. For dispelling the correlation time, the electronic conductivity are evaluated for 15-20 selected snapshots taken from the QMD trajectory. The selected snapshots or configurations are spaced by at least the correlation time. A $4 \times 4 \times 4$ Monkhorst-Pack k point mesh [25] has been used to calculate the electronic structure. The dynamic conductivity is derived from the Kubo-Greenwood formula as follows [17,18]:

$$\sigma_1(\omega) = \frac{2\pi}{3\omega\Omega} \sum_{\mathbf{k}} W(\mathbf{k}) \sum_{j=1}^{N} \sum_{i=1}^{N} \sum_{\alpha=1}^{3} [f(\epsilon_i, \mathbf{k}) - f(\epsilon_j, \mathbf{k})]$$
$$\times |\langle \Psi_{j,\mathbf{k}} | \nabla_\alpha | \Psi_{i,\mathbf{k}} \rangle|^2 \delta(\epsilon_{j,\mathbf{k}} - \epsilon_{i,\mathbf{k}} - \hbar\omega), \quad (1)$$

where $\Psi_{i,\mathbf{k}}$ is the Kohn-Sham eigenstate, with corresponding eigenvalue $\epsilon_{i,\mathbf{k}}$ and occupation number $f(\epsilon_i, \mathbf{k})$. Ω is the volume of the supercell. $W(\mathbf{k})$ is the K-point weighting factor. The i and j summations range over N discrete bands included in the calculation and α over the three spatial directions.

The imaginary part of conductivity σ_2 is obtained via the Kramers-Kronig relation as

$$\sigma_2(\omega) = -\frac{2}{\pi} P \int \frac{\sigma_1(\nu)\omega}{(\nu^2 - \omega^2)} d\nu, \quad (2)$$

where P is the principal value of the integral and ν is frequency. The complex dielectric function ϵ follows immediately from

the two parts of the conductivity by the following equations

$$\epsilon_1(\omega) = 1 - \frac{4\pi}{\omega}\sigma_2(\omega); \quad \epsilon_2(\omega) = \frac{4\pi}{\omega}\sigma_1(\omega). \quad (3)$$

The real part $n(\omega)$ and the imaginary part $k(\omega)$ of the refraction index have the following relation with the dielectric function

$$\epsilon(\omega) = \epsilon_1(\omega) + i\epsilon_2(\omega) = [n(\omega) + ik(\omega)]^2. \quad (4)$$

From these quantities, the absorption coefficient $\alpha(\omega)$ and reflectivity $r(\omega)$ are derived

$$\alpha(\omega) = \frac{4\pi}{n(\omega)c}\sigma_1(\omega), \quad (5)$$

$$r(\omega) = \frac{[1 - n(\omega)]^2 + k(\omega)^2}{[1 + n(\omega)]^2 + k(\omega)^2}. \quad (6)$$

III. RESULTS AND DISCUSSIONS

A. Equation of state and structure

The EOS has shown a systematic behavior in terms of density and temperature. As has been reported previously, at temperatures between 3 000 and 4 000 K along the principal Hugoniot, the dissociation of methane occurs and nonmetal-metal phase transition takes place simultaneously [5]. As a consequence, we have studied the thermal EOS of fluid ethane along 3 000, 4 000, and 8 000 K isotherms, as shown in Table I. The pressure P consists of two components P_e and P_i. The gradient of total energy calculated by VASP determines P_e, which represents the contributions from ion-ion, ion-electron, and electron-electron interactions. Due to the classical movement of ions, the ionic part P_i is derived by the ideal gas expression. We thus have $P = P_e + \rho_n K_B T$, where ρ_n is the number density. The simulated isotherm EOS for dense ethane is shown in Fig. 1. We have fitted the simulated results for the pressure P by expansions in terms of density ρ and temperature T as following $P = \sum A_{ij}\rho^i T^j$. The coefficients A_{ij} are listed in Table II. This expansion can
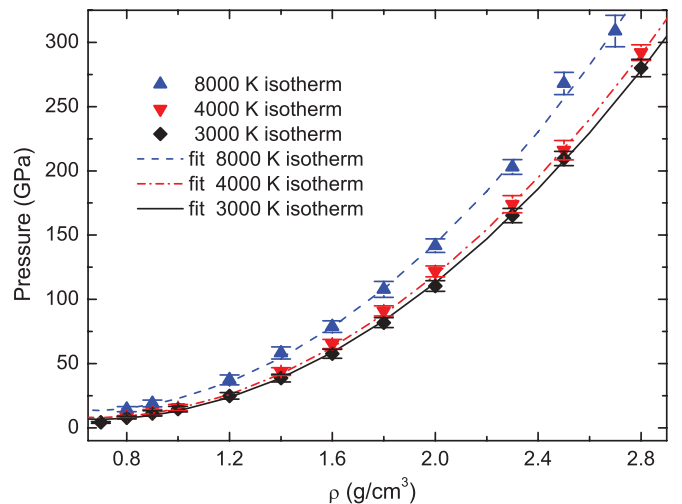

FIG. 1. (Color online) Pressure versus density along three isotherms ($T = 3\,000$, $4\,000$, and $8\,000$ K). The lines are fitting of the simulation results along isotherms.

TABLE I. The simulated data of the density, pressure, and the standard deviation of pressure.

ρ (g/cm^3)	T (K)	P (GPa)	ΔP (GPa)
0.80	3 000	7.94	1.04
0.90	3 000	11.24	2.05
1.00	3 000	14.57	2.21
1.20	3 000	24.84	2.54
1.40	3 000	38.72	2.99
1.60	3 000	57.66	3.49
1.80	3 000	81.86	3.91
2.00	3 000	110.38	4.20
2.30	3 000	165.22	5.60
2.50	3 000	209.59	5.58
2.80	3 000	280.04	6.72
0.80	4 000	8.54	1.07
0.90	4 000	11.90	2.41
1.00	4 000	15.78	2.39
1.40	4 000	43.79	3.03
1.60	4 000	65.24	3.50
1.80	4 000	91.06	3.98
2.00	4 000	121.69	4.24
2.30	4 000	174.01	6.69
2.50	4 000	216.11	7.48
2.80	4 000	294.00	6.12
0.80	8 000	14.50	1.93
0.90	8 000	18.96	2.72
1.20	8 000	37.32	3.86
1.40	8 000	58.22	4.69
1.60	8 000	78.84	4.50
1.80	8 000	107.73	6.17
2.00	8 000	141.75	5.25
2.30	8 000	203.00	5.72
2.50	8 000	268.07	8.67
2.70	8 000	308.87	12.26

easily be applied in hydrodynamic simulations for warm dense ethane in astrophysical applications.

To clarify the structural transitions of ethane under extreme conditions, we have calculated the pair-correlation functions (PCFs), which represent the possibility of finding a particle at a distance r from a reference atom. The PCFs and the atomic structure together with charge density distributions along 3 000 K isotherm are presented in Figs. 2 and 3, respectively. At the low density $\rho = 1.60$ g/cm^3, the peak in the C-H PCF $g_{C-H}(r)$ exists at around 1.09 Å [Fig. 2(a)], which is the equilibrium internuclear distance of the C-H bond in ethane molecule. Meanwhile, the peak in the C-C PCF $g_{C-C}(r)$ occurs at the equilibrium internuclear distance of C-C bond of saturated hydrocarbon (1.54 Å). Therefore, below the density of 1.60 g/cm^3, ethane remains in its ideal molecular configuration without dissociation. From the

TABLE II. Pressure (GPa) expansion coefficients A_{ij} in terms of density (g/cm^3) and temperature (K).

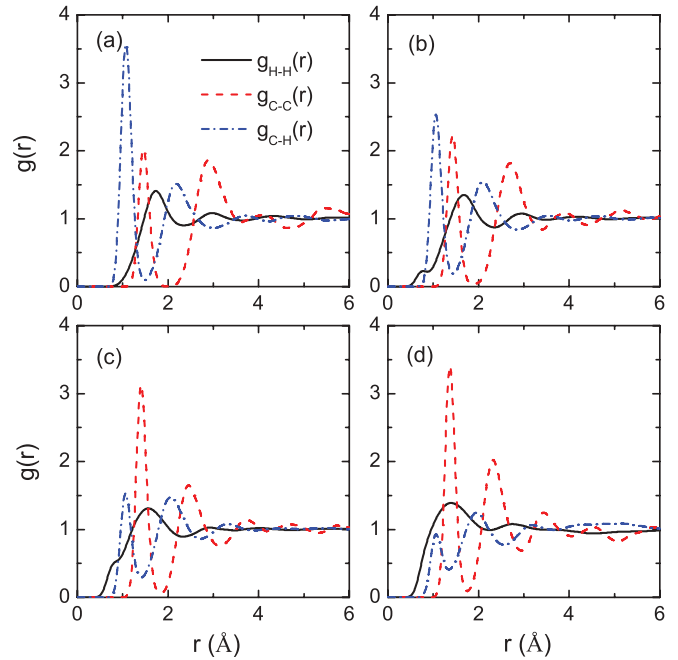| j	A_{0j}	A_{1j}	A_{2j}
0	27.3780	−73.3830	53.4723
1	0.0017	−0.0018	0.0020

FIG. 2. (Color online) Pair-correlation functions for H-H (black solid line), C-C (red dashed line), and C-H (blue dashed dot line) for four densities of dense ethane along 3 000 K isotherm. (a) $\rho = 1.60$ g/cm^3; (b) $\rho = 2.00$ g/cm^3; (c) $\rho = 2.30$ g/cm^3; (d) $\rho = 2.80$ g/cm^3.

structure of ethane at 1.60 g/cm^3 [Fig. 3(a)], we can straightly find that all of the ethane molecules are not dissociated. At the density of 2.00 g/cm^3, we find a significant reduction of the maximum of $g_{C-H}(r)$ around 1.09 Å, which indicates that the C-H bond breaks rapidly and ethane molecules dissociate with the increase of the density. On the other hand, around 0.75 Å a shoulder appears in the H-H PCF at this density, which implies the formation of molecular hydrogen. As the density further increases to 2.3 g/cm^3, the maximum of the PCF $g_{C-H}(r)$ continues to reduce while the peak amplitudes in $g_{C-C}(r)$ increases, which indicates that ethane further dissociates into some hydrocarbons. From Fig. 3(c), we can see that a new species of long alkane chains show up in the atomic configuration, corresponding to the increase of the peak of $g_{C-C}(r)$. More hydrogen molecules forms at this density, which corresponds to the larger value of $g_{H-H}(r)$ around 0.75 Å. Note that hydrogen molecules or atoms appear much more in Fig. 3(c) than in Fig. 3(b). However, the peak of $g_{H-H}(r)$ around 0.75 Å gets less apparent, and even vanishes at 2.8 g/cm^3. This may be because that (i) the peak of $g_{H-H}(r)$ around 0.75 Å are covered by the widening of the peak around the distance between the two hydrogen atoms bonding with a carbon atom (i.e., more complicated alkane structures and more hydrogen molecules and atoms form); and/or (ii) the formed hydrogen molecules partially dissociated into hydrogen atoms.

From the reported of Li *et al.* [5], it is known that above the density 1.05 g/cm^3 along the Hugoniot curve (above the pressure 25 GPa), methane begins dissociate and leads to the appearance of ethane and some linear carbon chains. In our study on the PCF of ethane, we find that ethane begins to
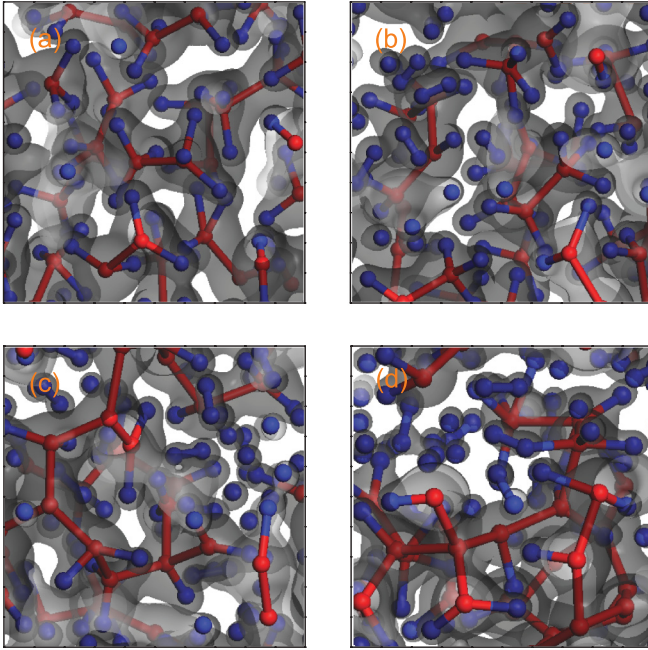
FIG. 3. (Color online) The atomic structure and charge density distribution of dense ethane at four density along 3000 K isotherm. Carbon and hydrogen atoms are denoted by red and blue balls, respectively. (a) $\rho = 1.60$ g/cm^3; (b) $\rho = 2.00$ g/cm^3; (c) $\rho = 2.30$ g/cm^3; (d) $\rho = 2.80$ g/cm^3.
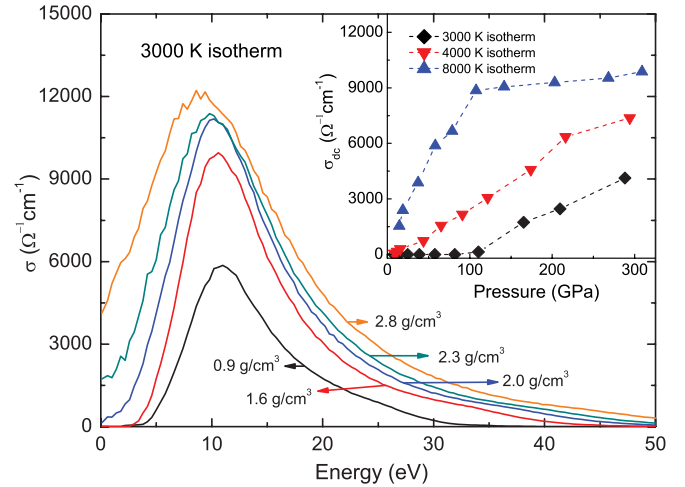

FIG. 4. (Color online) Optical conductivity spectra along the 3000 K isotherm. Data have been averaged over 15–20 uncorrelated MD configuration. The dc conductivities as a function of density along 3000, 4000, and 8000 K isotherms have been shown in inset.

dissociate at the pressure 81 GPa, and hydrogen and alkane chains form. Compared with the dissociation of methane at warm dense region [5], both of the hydrocarbons have the similar dissociation behavior with increase of the density. The dissociated products of both alkane species are hydrogen and alkane chains. Therefore, starting at methane or ethane should result in basically the same final state comprising alkane chains and hydrogen molecules and atoms at high enough pressures and temperatures, except for the quantity of alkane chains and molecular or atomic hydrogen. In addition, in the whole dissociation process of ethane and methane simulated theoretically, no diamond is formed, whereas it was experimentally reported that the diamond is formed at pressure $P = 20$ GPa and temperature $T = 2000$ K for methane [1]. Richters *et al.* [4] have employed a homogenous nucleation mechanism, which is similar to the proposal of the direct graphite-to-diamond transition [26,27], to explain the discrepancy between theory and experiment for methane.

B. Optical and electronic properties

We have calculated the electronic conductivity and corresponding reflectivity of fluid ethane along isotherms by Kubo-Greenwood formula. The behavior of the frequency-dependent conductivity $\sigma_1(\omega)$ at different densities along 3000 K isotherms is shown in Fig. 4. It has been found that $\sigma_1(\omega)$ at these four different densities exhibit a uniform feature that their peaks all locate around 10.0 eV, which is correlated with the transitions to the lowest excited states. With the increase of density along isotherm, the main peak of the electrical conductivity $\sigma_1(\omega)$ increases in amplitude and moves to low frequency. Such change of the peak indicates

another quantity, dc conductivity, given as $\sigma_{dc} = \lim_{\omega \to 0} \sigma_1(\omega)$, increases with density. The dc conductivity is extracted from dynamic conductivity and shown in the inset of Fig. 4. The dc conductivity σ_{dc} at low density along 3000 K isotherm is small, which corresponds to the character of a semiconductor [28,29]. With increasing density, the dc conductivity σ_{dc} increases rapidly. Above 2.30 g/cm^3 ($P = 165$ GPa), a metal-like conductivity is found. In order to analyze the effect of temperature on the nonmetal-metal transition, we have also shown the dc conductivity along higher temperature 4000 and 8000 K isotherms in Fig. 4. At low density and high temperature the dc conductivity can also reach a large value, which is a typical character of metallic behavior.

Mott *et al.* [30] have reported a decisive physical assertion, which is used to define the metallicity of a disordered system. When the characteristic mean free path of the valence electrons exceeds the mean distance between the constituent atoms or molecules, the states in disordered system with
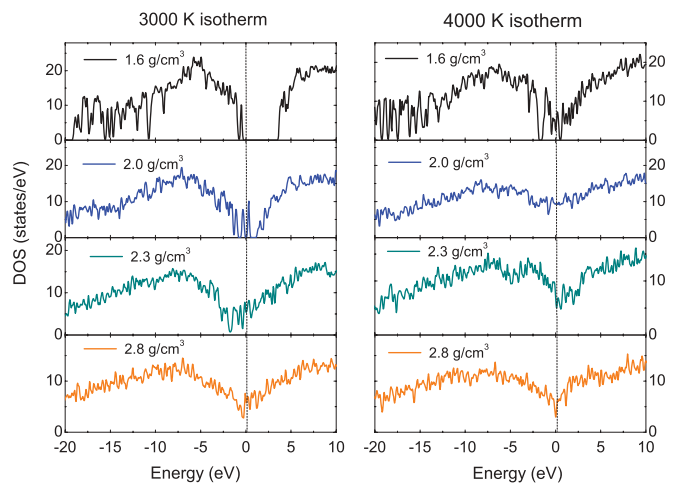

FIG. 5. (Color online) The density of state of fluid ethane at four different density points along 3000 K isotherm. The Fermi energy is set to be zero.
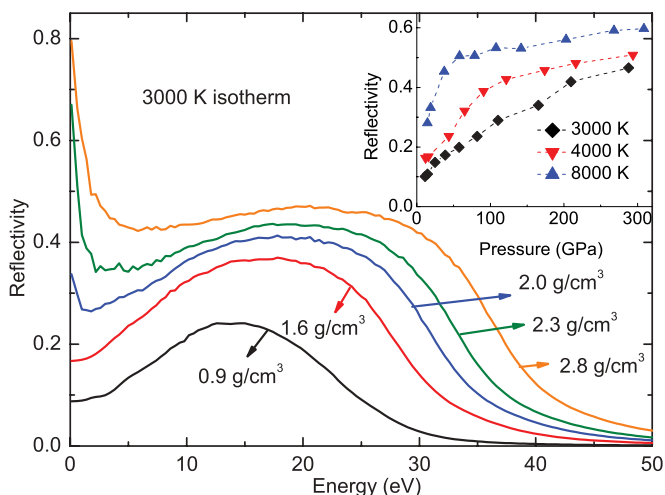
FIG. 6. (Color online) Variation of the frequency-dependent reflectivity $r(\omega)$ along 3 000 K isotherm. variation of the reflectivity as a function of density at fixed wavelengths of 404 nm along 3 000, 4 000 and 8 000 K isotherms.

any high-temperature will remain metallic or indeed attain metallic status. The constituent atoms or molecules provide the carriers of the electrical current. Applying Mott's criterion for the minimum electrical conductivity for fluid metals, the minimum electrical conductivity is about 1 000 $\Omega^{-1}cm^{-1}$ for fluid hydrogen, rubidium, caesium, and mercury [31]. The NMT has recently been observed in the nominally nonmetallic chemical elements hydrogen, nitrogen, and oxygen under extreme conditions [31,32].

At high pressures, materials undergo dissociation exhibiting some interesting properties. For instance, the band gap between the valence and conduction bands decreases with pressure and then disappears. The NMT has close relation with the molecular dissociation in the shocked fluid. In the case of fluid hydrogen and methane, QMD simulations have suggested that high-pressure NMT and the dissociation of molecules with increasing pressure are closely connected [5,33]. The dissociated atoms act as dopants and progressively occupy the dense-fluid band gap. In order to validate this physical picture, we have calculated the various electron density of states at different densities along 3 000 and 4 000 K isotherms as shown in Fig. 5. For the low density 1.60 g/cm^3, a gap exits, locating near the Fermi energy where only thermally activated electron transport occurs, which is exactly the situation in semiconductors or nonmetals. With increasing the density, the gap is gradually reduced and finally disappears. At density

2.30 g/cm^3, the electronic states fill up the gap so that metal-like conductivity follows. In addition, Compared with the same density along different isotherm, we can see the temperature effect on the electronic structure. Such effect can also be visualized in the dc conductivity σ_{dc}-pressure plotted in the inset of Fig. 4.

The optical reflectivity versus photon energy at different densities along the 3 000 K isotherm is shown in Fig. 6 (the main panel). With the increase of density along the isotherm, the reflectivity asymptotically approaches unity for zero photon energy. The reflectivity versus density at fixed wavelength 404 nm (corresponding to 3.075 eV) of fluid ethane along the 3 000, 4 000, and 8 000 K isotherms have been shown in the inset of Fig. 6. As is seen, a measurable reflectivity arises from 0.10 to 0.49–0.59 at typical wavelength of 404 nm spanning the visible spectrum, which is related with the high-pressure NMT. Similar behavior in the optical reflectance of fluid methane has been obtained by using QMD simulations [5]. The results of the optical reflectivity can be inspected through future experiments, and the reflectivity of liquid deuterium has been executed in experiment [11].

IV. CONCLUSIONS

In summary, first-principles molecular-dynamics simulations based on density-functional theory have been used to study the thermal EOS and nonmetal-metal transition of fluid ethane under extreme conditions. Systematic descriptions of pair-correlation function, atomic structure, and the charge density distribution with various densities along the isotherms are obtained to show the dissociation process of molecular fluid ethane, which is associated with the nonmetal-metal transition. Ethane dissociate with increasing the density and temperature into molecular and/or atomic hydrogen and some long alkane chains, which is similar to the case of methane. However, no diamond-like carbon microstructure is observed for ethane under extreme condition, the present result shows a different high pressure behavior compared with previous experiments. The nonmetal-metal transition has significant influence on the optical properties of fluid ethane, which needs to be verified in dynamic compression experiments. Our results are expected to be revealing for the planetary models of Neptune.

[1] L. R. Benedetti, J. H. Nguyen, W. A. Caldwell, H. J. Liu, M. Kruger, and R. Jeanloz, Science **286**, 100 (1999).

[2] S. Stanley and J. Bloxham, Icarus **184**, 556 (2006).

[3] S. Stanley and J. Bloxham, Nature (London) **428**, 151 (2004).

[4] D. Richters and T. D. Kühne, arXiv:1206.4500v1.

[5] D. Li, P. Zhang, and J. Yan, Phys. Rev. B **84**, 184204 (2011).

[6] G. Gao, A. R. Oganov, Y. Ma, H. Wang, P. Li, Y. Li, T. Lilaka, and G. Zou, J. Chem. Phys. **133**, 144508 (2010).

[7] J. de Vries, J. M. Hall, S. L. Simmons, M. J. A. Rickard, D. M. Kalitan, and E. L. Petersen, Combust. Flame **150**, 137 (2007).

[8] Y. Hidaka, K. Sato, H. Hoshikawa, T. Nishimori, R. Takahashi, H. Tanaka, K. Inami, and N. Ito, Combust. Flame **120**, 245 (2000).

[9] D. G. Friend, H. Ingham, and J. F. Ely, J. Phys. Chem. Ref. Data **20**, 275 (1991).

[10] C. Wang and P. Zhang, J. Appl. Phys. **107**, 083502 (2010).

[11] P. M. Celliers, G. W. Collins, L. B. Da Silva, D. M. Gold, R. Cauble, R. J. Wallace, M. E. Foord, and B. A. Hammel, Phys. Rev. Lett. **84**, 5564 (2000).

[12] T. J. Lenosky, S. R. Bickham, J. D. Kress, and L. A. Collins, Phys. Rev. B **61**, 1 (2000).

[13] L. Collins, I. Kwon, J. Kress, N. Troullier, and D. Lynch, Phys. Rev. E **52**, 6202 (1995).

[14] D. Hohl, V. Natoli, D. M. Ceperley, and R. M. Martin, Phys. Rev. Lett. **71**, 541 (1993).

[15] J. D. Kress, J. S. Cohen, D. A. Horner, F. Lambert, and L. A. Collins, Phys. Rev. E **82**, 036404 (2010).

[16] M. P. Desjarlais, J. D. Kress, and L. A. Collins, Phys. Rev. E **66**, 025401 (2002).

[17] R. Kubo, J. Phys. Soc. Jpn. **12**, 570 (1957).

[18] D. A. Greenwood, Proc. Phys. Soc. London **71**, 585 (1958).

[19] S. Mazevet, J. D. Kress, L. A. Collins, and P. Blottiau, Phys. Rev. B **67**, 054201 (2003).

[20] S. Mazevet, M. P. Desjarlais, L. A. Collins, J. D. Kress, and N. H. Magee, Phys. Rev. E **71**, 016409 (2005).

[21] G. Kresse and J. Hafner, Phys. Rev. B **47**, 558 (1993).

[22] G. Kresse and J. Furthmüller, Phys. Rev. B **54**, 11169 (1996).

[23] J. P. Perdew, K. Burke, and M. Ernzerhof, Phys. Rev. Lett. **77**, 3865 (1996).

[24] S. Nosé, J. Chem. Phys. **81**, 511 (1984).

[25] H. J. Monkhorst and J. D. Pack, Phys. Rev. B **13**, 5188 (1976).

[26] R. Z. Khaliullin, H. Eshet, T. D. Kühne, J. Behler, and M. Parrinello, Nat. Mater. **10**, 693 (2011).

[27] L. M. Ghiringhelli, C. Valeriani, J. H. Los, E. J. Meijer, A. Fasolino, and D. Frenkel, Mol. Phys. **106**, 2011 (2008).

[28] W. J. Nellis, S. T. Weir, and A. C. Mitchell, Science **273**, 936 (1996).

[29] W. J. Nellis, S. T. Weir, and A. C. Mitchell, Phys. Rev. B **59**, 3434 (1999).

[30] N. F. Mott, *Metal-Insulator Transitions*, 2nd ed. (Taylor and Francis, London, 1990).

[31] W. J. Nellis, J. Phys.: Condens. Matter **16**, 923 (2004).

[32] W. J. Nellis, R. Chan, P. P. Edwards, and R. Winter, Z. Phys. Chem. **217**, 795 (2003).

[33] L. A. Collins, S. R. Bickham, J. D. Kress, S. Mazevet, T. J. Lenosky, N. J. Troullier, and W. Windl, Phys. Rev. B **63**, 184110 (2001).